



Reference device for calibration of radon exhalation rate measuring instruments and its performance

Wei-Gang Li¹ · De-Tao Xiao¹ · Zheng-Zhong He¹ · Xiang-Yuan Deng¹ · Shou-Kang Qiu¹

Received: 10 January 2023 / Revised: 12 April 2023 / Accepted: 3 June 2023 / Published online: 28 August 2023

© The Author(s), under exclusive licence to China Science Publishing & Media Ltd. (Science Press), Shanghai Institute of Applied Physics, the Chinese Academy of Sciences, Chinese Nuclear Society 2023

Abstract

Environmental radon emanates from the exhalation and release of soil, rocks, and building materials. Environmental radon contamination tracing and radon pollution prevention and control require the measurement of the radon exhalation rate on media surfaces. Reliable measurements of the radon exhalation rate cannot be achieved without regular calibration of the measuring instrument with a high-performance reference device. In this study, a reference device for the calibration of radon exhalation rate measuring instruments was developed using a diffusion solid radon source with a high and stable radon emanation coefficient, an integrated diffusion component composed of a plasterboard and a high-density wooden board, an air pressure balance device, a radon accumulation chamber, and a support structure. The uniformity and stability of the reference device were evaluated using the activated carbon- γ spectrum and open-loop method, respectively, to measure the radon exhalation rate. The reference device achieved different radon exhalation rates by using different activities of diffusion solid radon sources. Nineteen measurement points were regularly selected on the radon exhalation surface of the reference device, and the uniformity of the radon exhalation rate exceeded 5%. The short-term stability of the reference device was better than 5% under different environmental conditions and was almost unaffected by the ambient air pressure, environmental temperature, and relative humidity.

Keywords Radon exhalation rate · Stability · Uniformity · High-density wooden board · Plasterboard

1 Introduction

Radon, a naturally occurring radioactive gas produced by the radioactive decay of ^{226}Ra [1], is the second leading cause of lung cancer after smoking [2] and was listed among the 19 most carcinogenic substances by the World Health Organization in 2009 [3]. Researchers have become increasingly interested in environmental radon exhalation rates (RERs) from media surfaces [4]. The RER is the radioactivity of radon exhaled from a media surface per unit area and time. In evaluating the efficacy of anti-radon coverage treatment in decommissioned uranium mines and metallurgy

facilities, such as waste rock yards and tailings reservoirs, RER measurements are essential [5, 6]. Additionally, source term inversion and radiation field reconstruction are crucial in alleviating environmental radon pollution [7]. Accurate RER measurements help determine the contribution of radon release to air pollution [8]. China has issued a standard (GB 50325-2020) for indoor environmental pollution control in civil building engineering [9], requiring that the measurement of the RER of building materials and the soil surface be performed continuously for 10 h using a monitor with a detection limit of less than $1 \text{ mBq m}^{-2} \text{ s}^{-1}$. Thus, an RER reference device should be developed to achieve reliable measurements of radon exhalation rates.

Researchers have been endeavoring to develop an RER reference device that achieves stability and uniformity and is almost unaffected by ambient air pressure, environmental temperature, and environmental relative humidity. Many RER measurement methods and devices have been developed [10–13]. However, the RER results measured by different monitors on the surface of the same media have

This work was supported by the National Natural Science Foundation of China (No.11875165).

✉ De-Tao Xiao
xiaodt@usc.edu.cn

¹ School of Nuclear Science and Technology, Hunan Provincial Key Laboratory of Radon, University of South China, Hengyang 421001, China

significantly differed, and the performance parameters have been inconsistent. In 1983, in the United States, Artley et al. [14] used a Bendix Company calibration device to track thin-source radon exhalation. The instrument verification efficiency of the RER was determined by deriving the tailing ejection coefficient and medium porosity from the theoretical design of the device. According to the verification results, the efficiency was higher than 100%. In 1990, the National Institute of Standards and Technology attempted to develop a standard device for measuring the RER. Colle et al. [15] developed a device composed of an electroplated solid radon source and plastic film that did not achieve a stable RER. In 1999, the University of South China developed a verification device for RER measuring instruments with satisfactory stability and uniformity [7]. The stability of the device used since 2000 was found to be significantly affected by changes in ambient air pressure. In 2015, Lv [16] measured the RER on the surface of a device by using the activated carbon- γ spectrum method. The RERs ranged from 1.34 to 2.03 $\text{Bq m}^{-2} \text{s}^{-1}$, and the uniformity was higher than 20% at 21 measurement points. In 2016, Tsapalov established a standard device that operates under ideal (laboratory environment) and nonideal (outdoor) conditions, providing a standard model for the nonideal case [17]. However, the observed and theoretical data significantly differed when the model was used for testing. Thus, increasing the accuracy of calibration devices is necessary to calibrate the various RER measuring instruments on the market and assess their performance parameters.

This study aimed to develop an RER reference device that exhibits short-term RER stability and uniformity better than 5%, rapidly adjusts the RER at different levels, and satisfies the calibration requirements of various instruments.

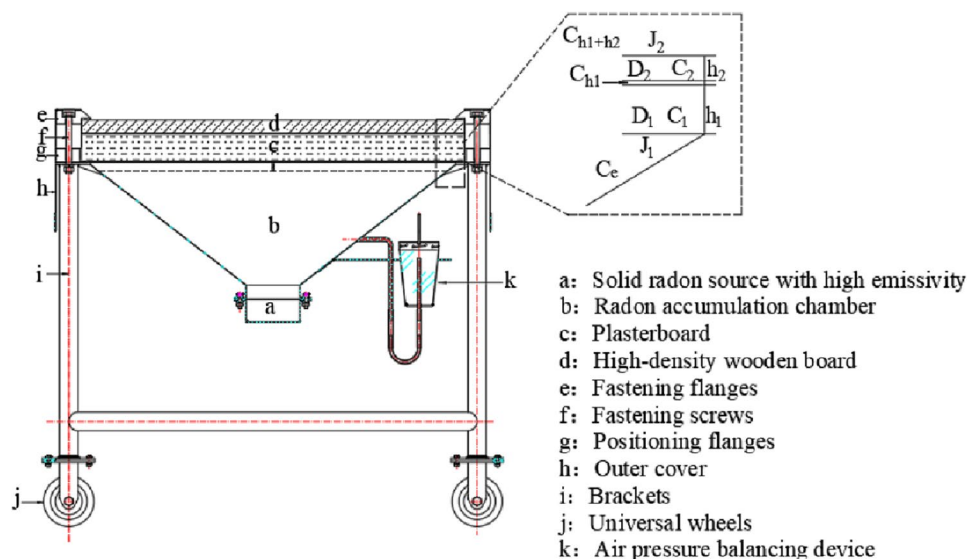
2 Material and methods

2.1 Architecture of RER reference device (RERRD)

Ambient air pressure influences radon migration, and the pressure gradient causes seepage [18]. Thus, dense and low-permeability double-layer plate materials were used as the diffusion media for the reference device, and an air pressure balance device was designed to reduce the influence of ambient air pressure.

As shown in Fig. 1, the RERRD comprises five parts. A 0.6 L cylindrical solid radon source chamber was located at the bottom of the RERRD. A solid radon source with a high emissivity coefficient, manufactured by the University of South China, was sealed inside a solid radon source chamber. This solid radon source had an emanation coefficient of $96 \pm 2\%$ under an ambient temperature of 10–45 °C and relative humidity of 40–90% [19–21]. The upper part of the solid radon source chamber was connected to an inverted radon accumulation chamber with a volume of 57.9 L. A pressure balance device containing a 95% saltwater mixture was installed at the bottom right of the radon accumulation chamber. For maintaining constant pressure inside and outside the RERRD, a U-shaped transparent organic glass tube connected the radon accumulation chamber to the ambient environment. The shifting effects of the radon accumulation chamber and external pressure during the migration process were due to the setting of the blue line on the surface of the glass tube. The diffusion of radon through the liquid into the environment was successfully stopped using a highly concentrated saltwater mixture. The high-humidity environment created at the mouth of the gas cylinder maintained a certain level of saltwater mixture concentration in the U-shaped tube, which reduced the diffusivity

Fig. 1 Schematic of the RERRD



of radon through the water body. The upper part of the radon accumulation chamber was designed with two crossbar support frames that could bear a load of approximately 300 kg. Diffusion media were placed on the upper part of the support frames. The high-density wooden board (thickness = 30 mm) and plasterboard (thickness = 60 mm) comprised cylindrical diffusion media with an inner diameter of 800 mm and an effective exhalation area of 0.5024 m². A stainless steel sheet was stamped and welded into one piece to form the shell of the device, with a total height of 0.6 m and a surface smoothness of less than 2 mm. The manufacturing company tested the airtightness of the device during factory delivery, and the device passed the test with satisfactory airtightness.

The radon accumulation chamber was formed as an inverted cone, and the diffusion media (plasterboard and high-density wooden board) were shaped into cylinders to guarantee a one-dimensional upward direction of radon diffusion. The plasterboard, created by an artificial combination of solidification and drying, had well-developed, unevenly distributed internal pores [22]. The high-density wooden board was fabricated using the high pressure of machines, and small and regular interior pores were formed. There is a crucial small pore between the plasterboard and the high-density wooden board. After the radon diffused through the plasterboard, it was evenly distributed in the pores. The radon evenly distributed in the pores diffuses to the surface through the high-density wooden board and finally forms a uniform RER. The plasterboard and high-density wooden board were combined at a specific thickness to ensure the stability and uniformity of the RER on the media surface. Surface moisture has a significant impact on the uniformity of the RERRD. The emulsion paint exhibited excellent waterproofing ability. The high-density wooden board coated with the paint emulsion was essentially moisture-free. The radon in the accumulation chamber was highly concentrated, and a concentration gradient existed between the upper and lower surfaces of the diffusion medium. Therefore, the radon exchange in the media occurs via active diffusion.

2.2 Principle of radon diffusion in a two-layered media

Radon exists as a single-atom gas at normal environmental temperatures, and its migration occurs via atomic thermal motion and convection. Because of the porous nature of the media, radon atoms can move freely through the connecting pores inside the media and diffuse out of the surface. The diffusion motion of radon in porous media obeys Fick's first law [23] is as follows:

$$J = -D \cdot \nabla C, \quad (1)$$

where J is the RER on the surface of the RERRD (Bq m⁻² s⁻¹), D is the radon diffusion coefficient in the

media (cm² s⁻¹), and ∇C is the radon concentration gradient in the media.

The second-order differential equation [24] for the diffusion and migration of radon through the medium is expressed by Eq. (2).

$$\frac{\partial C(x, t)}{\partial t} = D \frac{\partial^2 C(x, t)}{\partial x^2} - \lambda C(x, t), \quad (2)$$

where x denotes the coordinate of the axis normal to the surface of the medium (m).

The radon diffusion coefficient expresses the degree of radon diffusion in a medium. The relationship between the RER of the medium and the diffusion coefficient [25] is expressed by Eq. (3).

$$J = -D \frac{\partial C}{\partial x}. \quad (3)$$

When there is no pressure gradient in the surrounding space, the radon transport within the double-layer media is purely diffusion transport. Based on radon diffusion theories, when the radon concentration reaches a stable equilibrium state in space, the differential equation for radon diffusion in double-layer media is

$$\begin{cases} D_1 \frac{d^2 C_1}{dx^2} - \lambda C_1 = 0 \\ D_2 \frac{d^2 C_2}{dx^2} - \lambda C_2 = 0 \end{cases}, \quad (4)$$

where C_1 is the radon concentration in the plasterboard (Bq m⁻³), C_2 is the radon concentration in the high-density wooden board (Bq m⁻³), D_1 is the radon diffusion coefficient of the plasterboard (cm² s⁻¹), D_2 is the radon diffusion coefficient of the high-density wooden board (cm² s⁻¹), and λ is the radon decay constant (s⁻¹).

The ratio (k) between the RER on the lower surface of the plasterboard and that on the upper surface of the high-density wooden board was obtained as follows:

$$k = \frac{J_1}{J_2}, \quad (5)$$

where J_1 is the RER on the lower surface of the RERRD plasterboard, and J_2 is the RER on the upper surface of the high-density wooden board.

2.3 Methods for measuring RER

2.3.1 Instruments selection

Various instruments were used in the experiments. The radon monitor used was an FYCDY-P30 produced by Hubei Fangyuan Environmental Protection Technology Co., Ltd. The constant air pump was manufactured by Schauenburg Technology. The radon collection hood, an integrated and

forged cylindrical stainless steel plate, had a steel plate thickness of 2 mm, an inner diameter of 280 mm, a capacity of 5.85 L, and a bottom area of 0.06 m² (Fig. 2). The activated carbon boxes, made by the Beijing Institute of Metrology, were flat aluminum cylindrical boxes containing 80 g activated carbon. The thickness of the carbon layer was 2.5 cm and was covered with a metal screen and sealing cap. The sampling area of the activated carbon boxes was 3.848 × 10⁻³ m². The high-purity germanium gamma spectrometer was manufactured by the company ORTEC.

2.3.2 Open-loop method for measuring RER

The open-loop method was used to measure the RER [13], in which the radon collection hood was inverted on the surface of the exhalation media. The radon generated in the radon collection hood was pumped into the environment using the constant air pump. We wanted to ensure that the amount of radon pumped into the environment was equal to that generated from the surface of the media; thus, radon-free air was simultaneously added to the radon collection hood, which was connected to the FYCDY-P30 radon monitor. Radon-free air is produced by absorbing radon from the air through an activated carbon canister. After the RERRD reached an equilibrium state, the radon concentration was obtained from the alpha particle counts produced by the radon progeny decay electrostatically collected on the surface radon detector [26]. The variation with time of the radon concentration in the radon collection hood was expressed using Eq. (6).

$$\frac{dC}{dt} = \frac{J \cdot S}{V} - \lambda \cdot C - \frac{L(C - C_0)}{V} \tag{6}$$

When the radon concentration in the radon collection hood reaches a steady state, the left side of Eq. (6) is 0.

Then,

$$J = \frac{L(C - C_0)}{S} + \frac{\lambda \cdot V \cdot C}{S} \tag{7}$$

Because the natural decay constant of radon is 2.1 × 10⁻⁶ s⁻¹, (V·C)/S in Eq. (7) can be neglected, and Eq. (7) can be simplified to

$$J = \frac{L(C - C_0)}{S}, \tag{8}$$

where *J* is the RER to be measured on the surface of the exhalation media (Bq m⁻² s⁻¹), *L* is the flow rate of the constant air pump (L min⁻¹), *C*₁ is the radon concentration in the radon collection hood (Bq m⁻³), *C*₀ is the radon concentration in the environment (Bq m⁻³), *V* is the volume of the radon collection hood (m³), and *S* is the effective exhalation area of the radon collection hood (m²).

2.3.3 Activated carbon-γ spectrum method for measuring the RER

The activated carbon-γ spectrum method [27] was used to measure the RER from the surface of the reference device. The activated carbon boxes were placed upside down on the surface of the exhalation medium to collect the radon exhaled by the RERRD during sampling. A high-purity germanium gamma spectrometer was used to measure the intensities of the characteristic peaks of the radon daughters in the activated carbon. Finally, the activated carbon-γ spectrum method was used to obtain the RER. The selected coconut shell-activated carbon had significant radon adsorption properties. Therefore, the impact of leakage and counter-diffusion was minimal [28].

First, the activated carbon boxes were sealed immediately after sampling. In this case, the short-lived daughters of radon (²¹⁴Pb and ²¹⁴Bi) reached radioactive equilibrium with ²²²Rn [29]. This study used a high-purity germanium gamma spectrometer to measure the full energy peak area of the distinctive rays of the radon daughters; subsequently, the RER was calculated [10]. The 609 keV γ-rays from the decay of ²¹⁴Bi exhibited the highest branching ratio, the best energy peak shape, and least interference from other nuclides; thus, 609 keV γ-rays are generally used for experimental measurements [30].

To compare the results of multiple measurements, we selected a fixed area to measure the RER on the RERRD surface. Nineteen activated carbon boxes were evenly arranged in concentric circles on the surface of the exhalation media. Furthermore, these activated carbon boxes were used for

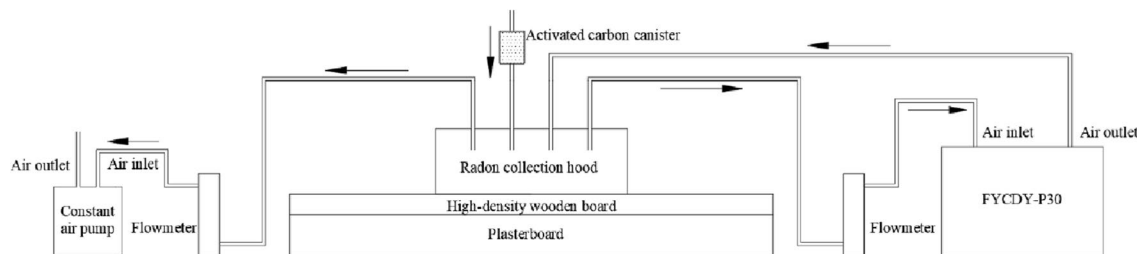


Fig. 2 Schematic of connection using open-loop method

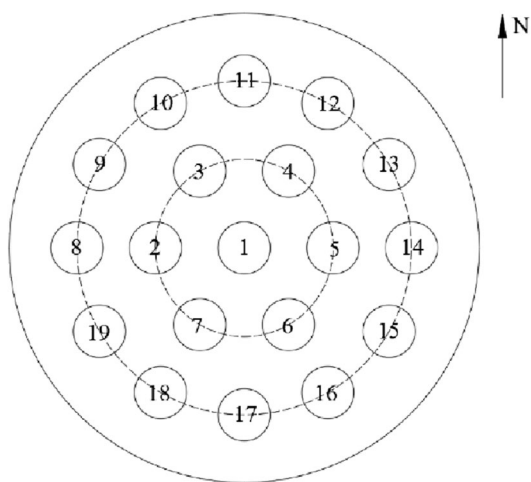


Fig. 3 Schematic of the points of activated carbon boxes

measurements and distributed uniformly over the surface of the exhaled media. A schematic of the points on the activated carbon boxes is shown in Fig. 3. The activated carbon boxes were dried at 120 °C for 8 h before the experiment. The background counting rate of the activated carbon boxes was measured after cooling, and the boxes were inverted equally on the surface of the exhaling media. The borders of the activated carbon boxes were sealed with plastic and stored for 24 h. The high-purity germanium gamma spectrometer was used to measure the net count rate after 3 h. The RERs were measured three consecutive times and calculated using Eq. (9).

$$J = \frac{(n_r - n_b) \lambda \cdot e^{\lambda T}}{K \cdot S(1 - e^{-\lambda T_s})} \tag{9}$$

where J is the RER on the surface of the media to be measured ($\text{Bq m}^{-2} \text{s}^{-1}$), K is the scale factor of the high-purity germanium gamma spectrometer for 609 keV energy gamma rays (the scale factor was applied to the standard source scale before use) ($0.007 \text{ cps Bq}^{-1}$), n_r is the full energy peak area (net count rates) of the characteristic 609 keV gamma rays (cps), n_b is the background counting rate of the activated carbon before the sampling rate (cps), S is the bottom area of the activated carbon boxes (m^2), T_s is the sampling time (h), λ is the decay constant of radon (s^{-1}), and T is the time interval between stopping sampling of the activated carbon boxes and the start of the high-purity germanium gamma spectrometer measurement (h).

The uncertainty of the gamma spectrometry of the activated carbon- γ spectrum method mainly originates from the detection efficiency of the high-purity germanium gamma spectrometer and the uncertainty in the production process of the standard source. The high-purity germanium gamma spectrometer was calibrated using a 230 Bq standard source

before use. The relative uncertainty of the spectrometer was approximately 5%, and the uncertainty in the production process of the standard source was approximately 3%. Because of the uncertainty of the experiment, the overall uncertainty of this method can be controlled within 10% [10].

2.4 Methods for measuring the media radon diffusion coefficient

A miniaturized reference device was used to measure the radon diffusion coefficient of the medium (Fig. 4). The type of diffusion medium could be changed arbitrarily. The volume of the radon accumulation chamber was V_1 (m^3); the radon concentration in the radon accumulation chamber was C_1 (Bq m^{-3}); and the change in radon concentration exhaled from the media was measured continuously using the open-loop method. The volume of the radon collection hood was denoted as V_2 (m^3); the radon concentration in the radon collection hood was denoted as C_2 (Bq m^{-3}); the bottom area of the radon collection hood was denoted as S (m^2); and the thickness of the media was denoted as H (m).

Then,

$$\frac{C_2}{C_1} = \frac{S \cdot D}{\lambda \cdot H \cdot V_1} \left[1 + 2 \sum_{n=1}^{\infty} (-1)^n \times \frac{1}{1 + \frac{n^2 \pi^2 D}{\lambda \cdot H^2}} \right], \tag{10}$$

when D/H^2 is sufficiently large, Eq. (10) can be simplified to

$$D = \frac{\lambda \cdot H \cdot V_1 \cdot C_2}{S \cdot C_1}. \tag{11}$$

The radon diffusion coefficients of the plasterboard and high-density wooden board can be calculated using Eq. (11).

2.5 Method for rapidly establishing equilibrium radon concentration in radon accumulation chamber

Radon in the accumulation chamber was generated from solid radon sources, which required an excessively long time to reach equilibrium. As shown in Fig. 1, to rapidly establish

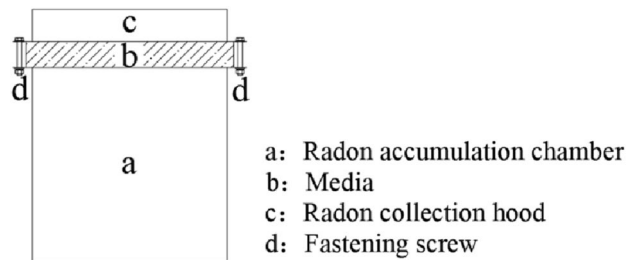


Fig. 4 Schematic of miniaturized reference device

the equilibrium radon concentration in the radon accumulation chamber, a method was adopted wherein the radon accumulation chamber was filled with a flowing gas–solid radon source in the initial state. The flowing gas–solid radon source must be emptied before use. The radon accumulation chamber was filled using an air pump after accumulation for a certain period. The variation in the radon concentration in the accumulation chamber is expressed by Eq. (12).

$$\frac{dC}{dt} = \frac{\lambda \cdot \eta \cdot A_0}{V} - \frac{J_1 \cdot S}{V} - \lambda \cdot C, \tag{12}$$

where A_0 is the activity of the flowing gas solid radon source (Bq), V is the volume of the radon accumulation chamber (m^3), C is the radon concentration in the radon accumulation chamber ($Bq\ m^{-3}$), J_1 is the RER on the lower surface of the plasterboard ($Bq\ m^{-2}\ s^{-1}$), S is the effective exhalation area (m^2), η is the solid radon source jet coefficient, and λ is the radon decay constant (s^{-1}).

When the radon concentration reaches the equilibrium state, the left side of Eq. (12) is equal to zero; thus, the initial radon concentration, denoted C_e , is obtained.

As $J_1 = k \cdot J_2$. Equation (12) is reduced to

$$C_e = \frac{1}{V} \left(\eta \cdot A_0 - \frac{k \cdot J_2 \cdot S}{\lambda} \right). \tag{13}$$

According to Eq. (13), when the activity of the solid radon source and the RER on the surface of the media are known, the initial radon concentration in the radon accumulation chamber can be obtained. The time required to attain equilibrium was reduced by the rapid filling of the radon accumulation chamber with a flowing gas solid radon source. Increasing the speed of the formation of a stable RER on the RERRD is feasible.

2.6 Methods for measuring uniformity and stability of RERRD

2.6.1 Uniformity measurement

The consistency of the RER at any location on the surface of the exhalation medium is indicated by the uniformity of the RERRD. The RERRD produced different RERs in the area used for each sampling event. Uniformity of the RERRD is necessary to ensure the accuracy of instrument calibration. The uniformity of the RERRD was indicated by a relative standard deviation of the RER of over 19 points. A smaller relative standard deviation indicated better uniformity of the RERRD.

The average RER over multiple points is

$$\bar{J}_1 = \frac{\sum_{i=1}^n J_i}{n}. \tag{14}$$

The uniformity of the RERRD is indicated by the relative standard deviation as follows:

$$u_r = \frac{1}{\bar{J}_1} \sqrt{\frac{\sum_{i=1}^n (J_i - \bar{J}_1)^2}{n(n-1)}} \times 100\%, \tag{15}$$

where u_r indicates the uniformity of the RERRD, J_i indicates the RER measured at point i ($Bq\ m^{-2}\ s^{-1}$), n is the number of measurement points, and \bar{J}_1 is the average RER over n points ($Bq\ m^{-2}\ s^{-1}$).

2.6.2 Short-term stability measurement

The short-term stability of RERRD indicates a change in its RER over a continuous period. The relative standard deviation of the measured RER was calculated by holding the radon collection hood upside down at the center of the exhalation medium and measuring the RER several times using the open-loop method.

The average of the multiple RER measurements is

$$\bar{J}_2 = \frac{\sum_{i=1}^n J_i}{n}. \tag{16}$$

The short-term stability of the RERRD is indicated by the relative standard deviation as follows:

$$\sigma = \frac{1}{\bar{J}_2} \sqrt{\frac{\sum_{i=1}^n (J_i - \bar{J}_2)^2}{n(n-1)}} \times 100\%, \tag{17}$$

where σ denotes the short-term stability of the RERRD, J_i denotes the RER of the central point measurement ($Bq\ m^{-2}\ s^{-1}$), n denotes the number of measurements, and \bar{J}_2 denotes the average RER over n measurements ($Bq\ m^{-2}\ s^{-1}$).

3 Results and discussion

3.1 Relationship between RERs on upper and lower surfaces of diffusion component

The diffusion coefficient of radon indicates its ability to migrate in media. After the radon concentrations in the radon accumulation chamber and the radon collection hood reached a dynamic equilibrium state, the diffusion coefficients of the media were calculated using Eq. (11). The radon diffusion coefficients of the plasterboard and high-density wooden board displayed in Table 1 are closely related to the RER on the upper and lower surfaces of the diffusion component.

As the diffusion coefficient decreased, the ability of radon to migrate in the medium weakened. As shown in Table 1,

the diffusion ability of radon on the plasterboard was lower than that on the high-density wooden board. Therefore, a high-density wooden board was placed atop the plasterboard in the double-diffusion media in the design of the RERRD.

On the basis of the data in Table 1, the radon diffusion coefficient of the plasterboard was denoted as D_1 ($2.94 \times 10^{-9} \text{ m}^2 \text{ s}^{-1}$), the radon diffusion coefficient of the high-density wooden board was denoted as D_2 ($1.42 \times 10^{-8} \text{ m}^2 \text{ s}^{-1}$), the thickness of the plasterboard was denoted as h_1 (0.06 m), the thickness of the high-density wooden board was denoted as h_2 (0.03 m). We analyzed k . By substituting D_1 , D_2 , h_1 , and h_2 into Eq. (4) and Eq. (5), we obtained

$$k = \frac{1}{14 \frac{C_{h_1+h_2}}{C_{h_1}} + 1} \tag{18}$$

The radon concentration exhaled from the RERRD on the surface of the high-density wooden board is much lower than that in the radon accumulation chamber, namely, $C_{h_1+h_2}/C_{h_1} \approx 0$; therefore, $k \approx 1$ and $J_1 \approx J_2$. The radon in the radon accumulation chamber was exhaled into the environment through the plasterboard and high-density wooden board. The RERs from the lower surface of the plasterboard and the upper surface of the high-density wooden board were approximately equal. In this case, a

Table 1 Radon diffusion coefficients for plasterboard and high-density wooden board

Media	Thick-ness H (m)	C_1 (Bq/m ³)	C_2 (Bq/m ³)	Diffusion coefficient D (m ² s ⁻¹)
Plasterboard	0.06	9813.64	763.03	2.94×10^{-9}
High-density wooden board	0.03	21,473.39	16,103.22	1.42×10^{-8}

solid radon source with different activities and RER can be rapidly obtained based on the initial radon concentration in the radon accumulation chamber by using Eq. (11). The time required for the RERRD to reach equilibrium can be reduced considerably from 28 days to approximately 2 days, which fulfills the requirements of experimental measurements rapidly.

3.2 Uniformity measurement result of the RER of the RERRD

The uniformity of the RER at any point on the surface of the diffusion medium is a crucial index for measuring the uniformity of the RERRD. The radon accumulation chamber of the RERRD was filled with two different solid radon sources with activities of 1.0×10^5 Bq and 2.0×10^5 Bq. The RER of the RERRD was measured thrice using the activated carbon- γ spectrum method. The measurement results are presented in Fig. 5.

The mean RERs at the 19 points were 197.78 ± 2.32 and $399.26 \pm 5.99 \text{ mBq m}^{-2} \text{ s}^{-1}$, and their relative standard deviations were 1.17% and 1.50%, respectively. The different points exhibited a uniformity of greater than 5%. The RERs measured at the points of the inner circle (2–7) swung up and down below the average. However, the RERs measured at points outside the circle (8–19) were higher than the average. The low efficiency of the high-purity germanium gamma spectrometer and the statistical errors in the measurement cannot be ignored. Another factor to consider is the latex paint sprayed on the surface of the high-density wooden board to eliminate the effects of moisture. Manual spraying could not ensure consistency in the thickness of the latex paint layer at each spot. The points with a thin latex paint layer had higher RERs than the other points did.

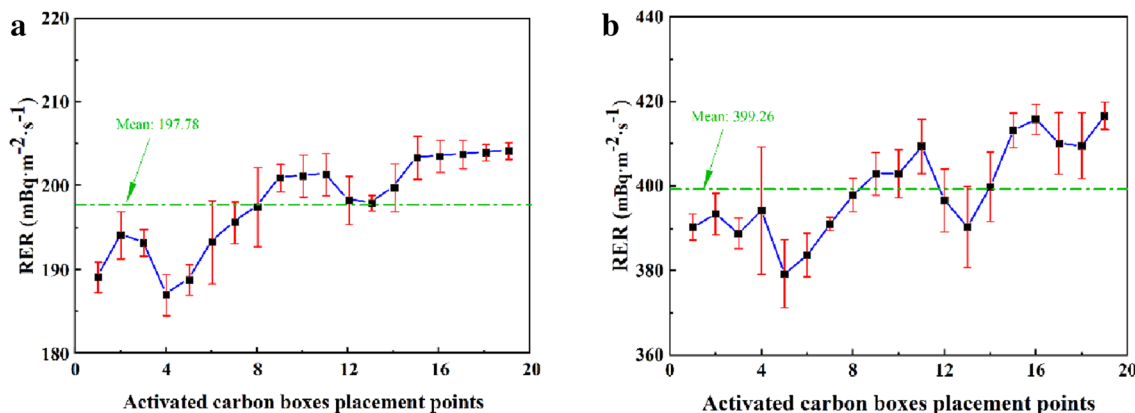


Fig. 5 (Color online) **a** Uniformity of RER after placing a 1.0×10^5 Bq solid radon source; **b** uniformity of RER after placing a 2.0×10^5 Bq solid radon source

3.3 Short-term stability measurement results of the RER of the RERRD

The short-term stability of the RER characterizes whether it is affected by changes in ambient air pressure, environmental temperature, relative humidity, and other conditions. The two solid radon sources with activities of 1.0×10^5 Bq and 2.0×10^5 Bq, respectively, were placed in the radon accumulation chamber. The radon collection hood was sampled and measured in the middle of the medium surface by using the open-loop method. The effects of the ambient pressure, environmental temperature, and relative humidity on the RER were studied.

3.3.1 Stability of the RER of the RERRD under various ambient air pressure

The temperature inside the room was controlled via air conditioning and maintained at 20 °C. The dehumidifier stabilized the relative humidity of the room at 40%. The hourly ambient air pressure and the RER were measured thrice using the open-loop method. The daily variation curves of ambient air pressure and the RER are shown in Fig. 6.

The ambient air pressure changed daily, with high values between 9 and 11 am and low values between 3 and 5 am [31]. By contrast, the RERs resulting from the solid radon sources of 1.0×10^5 and 2.0×10^5 Bq on the surface of the media of the RERRD varied little within 1 days, with daily relative standard deviations of 2.54% and 3.65%, respectively. Therefore, the short-term stability of the RERRD was greater than 4%. The pressure balance device of the RERRD can reduce the effects of ambient air pressure on radon migration. Internal changes in the

pressure in the radon accumulation chamber were maintained at all times. We calculated the correlation coefficient between the ambient air pressure and the radon exhalation rate and found that the correlation between these two factors was weak (Fig. 6a: 0.42; b: 0.35). The results revealed that the ambient air pressure had almost no effect on the RER of the RERRD.

3.3.2 Stability of the RER of the RERRD under various environmental temperatures

The environmental relative humidity was stabilized at 40% with a dehumidifier while imposing different environmental temperatures via air conditioning. As shown in Fig. 6, the influence of ambient air pressure on the RER, although nonsignificant, should be eliminated as much as possible. The open-loop method was used to conduct the experiment from 9:00 to 11:00 am daily. The relationship between the environmental temperature and the RER of the RERRD was measured thrice using the open-loop method (Fig. 7).

Figure 7 shows the relationship between the RER and environmental temperature at a relative humidity of 40% and essentially unchanged ambient air pressure. Because the adjustable range of the air conditioning is 16–30 °C, the temperature was set to 16 °C, 20 °C, 25 °C, and 30 °C, respectively; for a solid radon source with an activity of 1.0×10^5 Bq, the short-term stabilities were 1.02%, 0.76%, 1.52%, and 2.08%, respectively; by placing a solid radon source with an activity of 2.0×10^5 Bq, the short-term stability was 2.56%, 1.90%, 2.49%, and 4.14%, respectively. The short-term stability of the RERRD was within 5%. The environmental temperature had little effect on the RER of the RERRD.

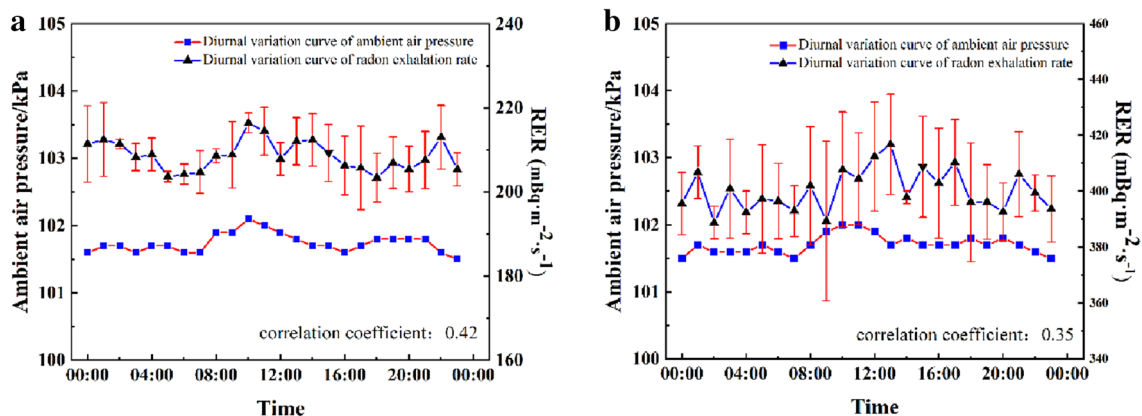


Fig. 6 (Color online) Variation in ambient air pressure and RER with time. **a** Daily variation curves of ambient air pressure and RER after placing a solid radon source with an activity of 1.0×10^5 Bq; **b** daily

variation curves of ambient air pressure and RER when placing a solid radon source with an activity of 2.0×10^5 Bq

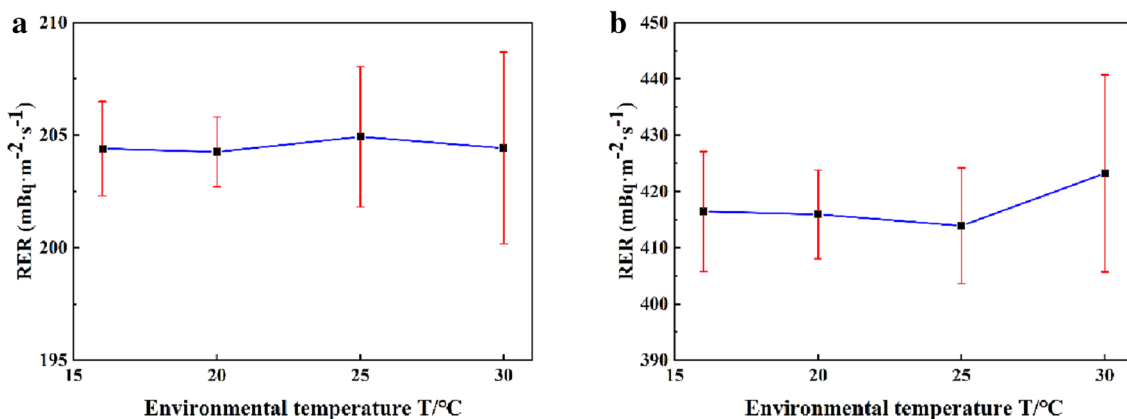


Fig. 7 Variation in RER with environmental temperature. **a** Relationship between RER and environmental temperature after placing a solid radon source with an activity of 1.0×10^5 Bq; **b** relationship

between RER and environmental temperature after placing a solid radon source with an activity of 2.0×10^5 Bq

3.3.3 Stability of the RER of the RERRD under various environmental relative humidity

First, the indoor air conditioning stabilized the temperature at 20 °C. Subsequently, a cloudy and rainy day (with high relative humidity in the environmental air) was selected. The relative humidity of the indoor air was controlled using a dehumidifier. To consider the influence of ambient air pressure, we used the open-loop method to conduct the experiment from 9:00 to 11:00 am. The effect of the environmental relative humidity on the RER of the RERRD is presented in Fig. 8.

The environmental temperature was 20 °C, and the ambient air pressure was essentially unchanged. The relationship between the RER and environmental relative humidity is shown in Fig. 8. When placing a solid radon source with an activity of 1.0×10^5 Bq, the relative humidity was set to 40%, 50%, 60%, 70%, 80%, and 90%; the short-term

stabilities were 1.97%, 1.78%, 2.54%, 2.40%, 2.37%, and 2.59%, respectively; for a solid radon source with an activity of 2.0×10^5 Bq, the short-term stabilities were 2.70%, 2.27%, 1.48%, 1.61%, 3.29% and 3.10%, respectively. The relative standard deviation and short-term stability of the RER of the RERRD were within 4% at $T = 20$ °C. The environmental relative humidity had little effect on the RER measurement, and it had almost no effect on subsequent measurements using the RERRD.

3.4 Relationship between activities of diffusion solid radon sources and the RER of the RERRD

The studied RERRD can create different levels of uniform and stable RERs on the surface of the media by changing the activities of the solid radon sources. The existing activities of the solid radon sources in the Radon Laboratory of the University of South China were 3.0×10^3 , 8.5×10^3 ,

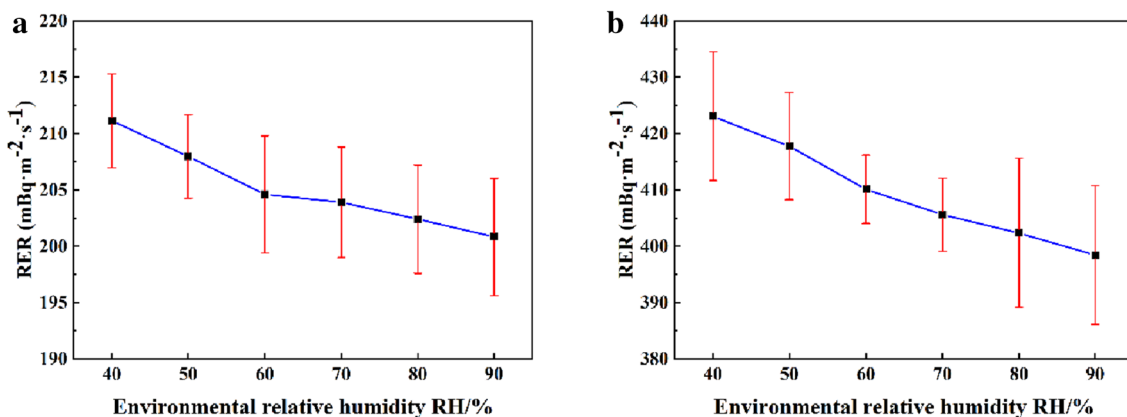


Fig. 8 **a** Relationship between RER and environmental relative humidity after placing a solid radon source with an activity of 1.0×10^5 Bq; **b** relationship between RER and environmental relative humidity after placing a solid radon source with an activity of 2.0×10^5 Bq

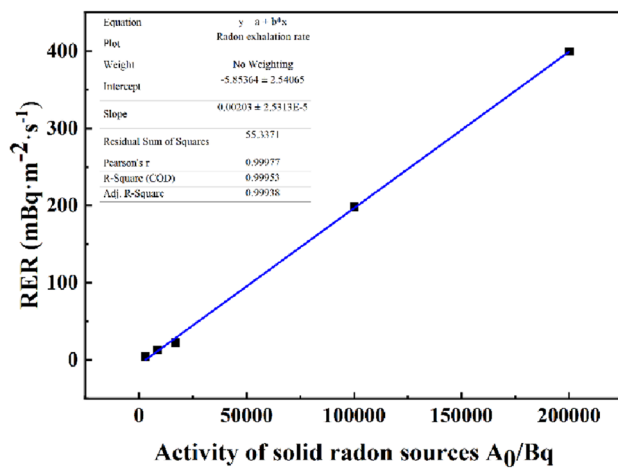


Fig. 9 Relationship between RERs and activities of solid radon sources

1.7×10^4 , 1.0×10^5 , and 2.0×10^5 Bq. They were placed separately in the accumulation chamber of the RERRD, and the RER was rapidly brought to a steady state by filling the accumulation chamber with a predetermined amount of radon. The activated carbon- γ spectrum method was used to measure the RER by placing solid radon sources with different activities at the midpoint of the medium. The results are shown in Fig. 9.

As shown in Fig. 9, a linear fitting equation between the RERs of the RERRD and the activities of the solid radon sources was obtained by linear fitting of the data as follows:

$$J = 0.002A_0 - 5.854. \quad (19)$$

Because the minimum activity of the solid radon source used in our experiment was 3000 Bq, Eq. (19) is valid when $A_0 \geq 3000$.

R^2 was 0.99. If the activity of a radon source placed in the RERRD is known, the RER of the RERRD can be rapidly obtained using Eq. (19). This finding provides a reference activity for a solid radon source for high RER levels and improves the experimental efficiency.

4 Conclusion

In this study, an integrated diffusion assembly was formed from a plasterboard and high-density wooden board using the solid radon sources of 3.0×10^3 , 8.5×10^3 , 1.7×10^4 , 1.0×10^5 , and 2.0×10^5 Bq, and an air pressure balancing device was developed to eliminate the influence of the ambient air pressure. The characteristics of RERRD were tested.

The uniformity of the RER on the surface of the media was less than 5% when solid radon sources with different

activities were inserted into the RERRD, and the short-term stability was less than 5%. The RER of the RERRD was almost unaffected by daily variations in ambient air pressure, environmental temperature, and environmental relative humidity. Therefore, the errors induced by these three factors can be disregarded. For calibration, the RERRD was set up in a laboratory under normal environmental conditions. If different RERs are required for an experiment, the activity of the solid radon source to be placed in the RERRD can be obtained rapidly. Moreover, the RERRD, designed as a detachable structure, allows experimental studies of RERs to be conducted by changing the diffusion media of different materials.

With excellent performance and rapid realization at various levels of RERs, the RERRD has the potential to be developed into a new type of calibration device for RER measuring instruments.

Acknowledgements We are particularly grateful to Drs. Shao-Bin Guan, Zong-Jie Zhou, Feng-Lin Li, and Tao Sun of the Chinese Nuclear Industry Remote Sensing Center for providing support under experimental conditions.

Author contributions All authors contributed to the study conception and design. Material preparation, data collection and analysis were performed by Wei-Gang Li, De-Tao Xiao, Zheng-Zhong He, Xiang-Yuan Deng and Shou-Kang Qiu. The first draft of the manuscript was written by Wei-Gang Li and all authors commented on previous versions of the manuscript. All authors read and approved the final manuscript.

Data availability The data that support the findings of this study are openly available in Science Data Bank at <https://doi.org/10.57760/sciencedb.j00186.00136> and <https://cstr.cn/31253.11.sciencedb.j00186.00136>.

Declarations

Conflict of interest The authors declare that they have no conflict of interest.

References

1. N. Lavi, V. Steiner, Z.B. Alfassi, Measurement of radon emanation in construction materials. *Radiat. Meas.* **44**(4), 396–400 (2009). <https://doi.org/10.1016/j.radmeas.2009.04.009>
2. United Nations Scientific Committee on the Effects of Atomic Radiation. Effects of Ionizing Radiation, United Nations Scientific Committee on the Effects of Atomic Radiation (UNSCEAR) 2006 Report, Volume I: Report to the General Assembly, Scientific Annexes A and B. United Nations, 2008. <https://doi.org/10.18356/7fb405cb-en>
3. D.-K. Ting, WHO handbook on indoor radon: a public health perspective. *Int. J. Environ. Stud.* **67**(1), 100–102 (2010). <https://doi.org/10.1080/00207230903556771>
4. Y. Huo, P. Xu, C. Zhou et al., Effect of environment humidity to radon measurement with SSNTD. *Nucl. Sci. Tech.* **20**(4), 228–230 (2009). <https://doi.org/10.13538/j.1001-8042/nst.20.228-230>

5. J. Somlai, Z. Gorjánác, A. Várhegyi et al., Radon concentration in houses over a closed Hungarian uranium mine. *Sci. Total Environ.* **367**(2–3), 653–665 (2006)
6. J. Jónás, J. Somlai, E. Tóth-Bodrogi et al., Study of a remediated coal ash depository from a radiological perspective. *J. Environ. Radioactiv.* **173**, 75–84 (2017). <https://doi.org/10.1016/j.jenvrad.2016.11.010>
7. X.J. Li, S.K. Qiu, C.K. Liu, A calibration facility for radon fluxmeter. *Radiat. Prot.* **28**(4), 197–201 (2008). (in Chinese)
8. S. Röttger, A. Röttger, C. Grossi et al., Radon metrology for use in climate change observation and radiation protection at the environmental level. *Adv. Geosci.* **57**, 37–47 (2022). <https://doi.org/10.5194/adgeo-57-37-2022>
9. P.Y. Wang, Y.F. Jia, Reduce indoor pollution and share fresh air—interpretation of GB 50325–2020 “Standard for door Environmental Pollution Control of Civil Building Engineering.” *Constr. Qual.* **39**(03), 1–5 (2021). (in Chinese)
10. L.D. Lv, Z.Z. He, S.K. Qiu et al., Evaluation and measurement methods for the surface radon exhalation rate of buildings. *Indoor Built Environ.* **31**(10), 2378–2385 (2022). <https://doi.org/10.1177/1420326X221109754>
11. Y.F. Yang, L.D. Lv, S.K. Qiu et al., Study on the influence of sampling methods for measuring soil radon exhalation rates. *Radiat. Meas.* **159**, 106880 (2022). <https://doi.org/10.1016/j.radmeas.2022.106880>
12. GB/T(Chinese Standards) GB/T 16143-1995. Charcoal canister method for measuring ^{222}Rn exhalation rate from building surface (English Vision). Beijing: National Health Commission of the People’s Republic of China, 1995.
13. Y.L. Tan, D.T. Xiao, H. Yuan et al., Revision for measuring radon exhalation rate in open loop. *J. Instrum.* **8**(01), T01004 (2013). <https://doi.org/10.1088/1748-0221/8/01/T01004>
14. J.N. Hartley, G.W. Gee, E.G. Baker, et al., 1981 Radon barrier field test at Grand Junction uranium mill tailings pile. Pacific Northwest Lab. Richland, WA (USA), 1983. <https://www.osti.gov/biblio/6405607>
15. R. Collé, J.M.R. Hutchinson, M.P. Unterweger, The NIST primary radon-222 measurement system. *J. Res. Natl. Inst. Stan.* **95**(2), 155 (1990). <https://doi.org/10.6028/jres.095.018>
16. L.D. Lv, X.P. Qiu, S.K. Qiu et al., Study of active carbon measuring method for accurate measurements of radon exhalation rates for building materials. *J. Univ. South China (Sci. Technol.)* **28**(01), 9–12 (2014). <https://doi.org/10.19431/j.cnki.1673-0062.2014.01.004> (in Chinese)
17. A. Tsapalov, K. Kovler, P. Miklyav, Open charcoal chamber method for mass measurements of radon exhalation rate from soil surface. *J. Environ. Radioactiv.* **160**, 28–35 (2016). <https://doi.org/10.1016/j.jenvrad.2016.04.016>
18. X.S. Liu, S.K. Qiu, A rapid and accurate method for measuring radon exhalation rate. *Radiat. Prot.* **27**(03), 156–162 (2007). <https://doi.org/10.3321/j.issn:1000-8187.2007.03.005> (in Chinese)
19. Q. Tang, S.K. Qiu, D.T. Xiao et al., Extraction and purification of ^{227}Ac and development of solid ^{219}Rn source. *Radiochim. Acta* **102**(1–2), 169–174 (2014). <https://doi.org/10.1515/ract-2014-2117>
20. J. Ke, Y.L. Ke, Y.H. Zhuang et al., The analysis of the performance in the calibration of radon measurement instrument by several kinds of solid standard source. *South China J. Seismol.* **35**(2), 43–49 (2015). <https://doi.org/10.13512/j.hndz.2015.02.007> (in Chinese)
21. W.Y. Du, GD—L2 Flow-type solid radon source calibration factors of radon measurement instrument and its influence. *J. Inst. Disaster Prev.* **15**(3), 67–71 (2013). <https://doi.org/10.3969/j.issn.1673-8047.2013.03.012> (in Chinese)
22. E. Saleh, A.M.A. Al-Sobahi, S.A.E. El-Fiki, Assessment of radon exhalation rate, radon concentration and annual effective dose of some building materials samples used in Yemen. *Acta Geophys.* **69**(4), 1325–1333 (2021). <https://doi.org/10.1007/s11600-021-00628-z>
23. M. Noguchi, H. Wakita, A method for continuous measurement of radon in groundwater for earthquake prediction. *J. Geophys. Res.* **82**(8), 1353–1357 (1977). <https://doi.org/10.1029/JB082i008p01353>
24. H.N.P. Thu, N. Van Thang, L.C. Hao, The effects of some soil characteristics on radon emanation and diffusion. *J. Environ. Radioactiv.* **216**, 106189 (2020). <https://doi.org/10.1016/j.jenvrad.2020.106189>
25. C. Miró, E. Andrade, M. Reis et al., Development of a couple of methods for measuring radon exhalation from building materials commonly used in the Iberian Peninsula. *Radiat. Prot. Dosim.* **160**(1–3), 177–180 (2014). <https://doi.org/10.1093/rpd/ncu063>
26. Z.Q. Li, D.T. Xiao, G.Z. Zhao et al., Rapid determination of radon monitor’s calibration factors. *Nucl. Sci. Tech.* **27**, 116 (2016). <https://doi.org/10.1007/s41365-016-0118-2>
27. P. Tuccimei, M. Moroni, D. Norcia, Simultaneous determination of ^{222}Rn and ^{220}Rn exhalation rates from building materials used in Central Italy with accumulation chambers and a continuous solid state alpha detector: influence of particle size, humidity and precursors concentration. *Appl. Radiat. Isot.* **64**(2), 254–263 (2006). <https://doi.org/10.1016/j.apradiso.2005.07.016>
28. G.P. Xiao, D.T. Xiao, L.D. Lv et al., Study on active carbon sampling device for measuring radon exhalation rate. *Nucl. Electron. Detect. Technol.* **35**(11), 1119–1123 (2015). <https://doi.org/10.3969/j.issn.0258-0934.2015.11.016> (in Chinese)
29. C.E. Lawrence, R.A. Akber, A. Bollhöfer et al., Radon-222 exhalation from open ground on and around a uranium mine in the wet-dry tropics. *J. Environ. Radioact.* **100**(1), 1–8 (2009). <https://doi.org/10.1016/j.jenvrad.2008.09.003>
30. S.H. Alharbi, R.A. Akber, Radon-222 activity flux measurement using activated charcoal canisters: revisiting the methodology. *J. Environ. Radioact.* **129**, 94–99 (2014). <https://doi.org/10.1016/j.jenvrad.2013.12.021>
31. J.L. Pinault, J.C. Baubron, Signal processing of diurnal and semi-diurnal variations in radon and atmospheric pressure: a new tool for accurate in situ measurement of soil gas velocity, pressure gradient, and tortuosity. *J. Geophys. Res. Solid Earth* **102**(B8), 18101–18120 (1997). <https://doi.org/10.1029/97JB00971>

Springer Nature or its licensor (e.g. a society or other partner) holds exclusive rights to this article under a publishing agreement with the author(s) or other rightsholder(s); author self-archiving of the accepted manuscript version of this article is solely governed by the terms of such publishing agreement and applicable law.